

# Active control for multi-degree-of-freedom wave energy converters with load limiting

Andrew J. Hillis, Craig Whitlam, Annette Brask, John Chapman and Andrew R. Plummer

## Abstract

An active control strategy is generated for multiple degree-of-freedom Wave Energy Converters (WECs). The purpose of the new control strategy is to maximise power capture across a range of seas whilst operating within physical system constraints. The WaveSub WEC is used as a target device with four rotational power take-offs (PTOs) attached to drums which are driven by taut tethers connected to a float. The full scale WEC has been modelled in the WEC-Sim environment using a fixed passive damping system for the PTOs, which was optimally tuned for individual sea states to provide a performance benchmark. An active control system utilising the simple and effective method with a Linear Quadratic Regulator velocity tracking loop is designed. A range of sea states is applied and the performance of the active and passive systems compared. Power gains of up to 80% are observed across a wide range of irregular sea states compared to the optimally tuned passive system. This approach shows significance in providing a substantial increase in power capture for a minimal additional device cost and therefore a major improvement in cost of energy would likely result.

*Keywords*—Active control, submerged Wave Energy Converter, power take off

## I. INTRODUCTION

1 Wave energy still faces many technological challenges on the path to commercialisation, with  
2 the over-arching challenge of reducing the cost of energy relative to other renewable sources.  
3 Nevertheless the potential resource is recognised as highly significant e.g. [1] and great efforts are  
4 being input to pursue the goal of affordable energy production with many new concepts under  
5 development. All WECs require a power take-off (PTO) to convert the wave input to useful electrical  
6 power. The PTO developer faces the challenges of designing systems that can extract energy efficiently  
7 from small waves whilst being able to survive high loading in extreme conditions. Many PTO designs  
8 are being explored and each has advantages and disadvantages. Classifications of PTO include direct  
9 drive electric, hydraulic and mechanical systems. Regardless of the PTO architecture, it must be  
10 controllable to maximise efficiency across the wide range of operating conditions it will experience.  
11 The control system can also be used to limit load transmission to aid survivability. It is generally  
12 accepted that the cost effective WEC and PTO will be highly utilised during the commonly occurring  
13 sea states and will shed load in higher sea states, approaching the ideal case termed the "100%  
14 sweating WEC" [2]. The control strategy is key to maximising this utilisation, and has its share of  
15 challenges.

16 Active control strategies may be targeted to achieve efficient power capture by keeping the velocity  
17 of the primary converter in phase with the wave excitation force. This may be achieved in an ideal  
18 manner through complex-conjugate control, for example see [3]. Practical implementation of complex-  
19 conjugate control is difficult as it is non-causal and can result in very large forces and motions of  
20 the device which could violate physical constraints. Alternative sub-optimal approaches have been  
21 proposed, for example latching and declutching control [4][5][6], which engage or disengage the PTO  
22 at a specified time. The disadvantage of these strategies is that they can result in large forces being  
23 transmitted to the WEC structure and PTO. Model Predictive Control (MPC) strategies have also  
24 been applied, see for example [7][8][9]. These have the advantage that physical constraints can be

incorporated, but the optimisation problem may be computationally intensive for a realistic nonlinear WEC and PTO making real-time implementation problematic [10]. Additionally, MPC depends on accurate plant models and requires prediction of the wave excitation which increases uncertainty and potentially reduces robustness. More recently pseudo-spectral control has been studied e.g. [11] and purports to have advantages over MPC in terms of computational burden and controlling nonlinear systems.

Many of these and similar studies are limited to idealised models of 1-DOF heaving buoys which are not representative of practical systems. Comparatively little attention has been paid to the control of multi-DOF systems. Abdelkhalik have studied the control of a 3-DOF floating point absorber which extracts power from heave, surge and pitch motion. They have applied various control strategies including optimal proportional-derivative [12] and pseudo-spectral control schemes [13]. In each case the benefits of large increases in power compared to extracting energy purely in heave have been shown. However, the target device is theoretical only, and no proposition for practical arrangements of PTO systems to achieve the control strategy are provided. Additionally, the system under control is assumed to be modelled precisely which may not be valid. This assumption is common to the majority of WEC control studies conducted in simulation. The Bristol cylinder is one example of a multi-DOF WEC which shares some features with the target device of this study - WaveSub under development by Marine Power Systems Ltd (MPS). It is a submerged tethered cylinder able to extract power from heave, surge and pitch motion [14]. More recently alternative arrangements have been explored [15] with a view to adding practicality to capturing the power. Control of the Bristol cylinder has been considered in [16], though this considers the power electronic hardware rather than active control strategies.

Many active control strategies require knowledge of the wave excitation force acting on the WEC and this is often assumed to be known precisely, even if forward prediction by several seconds is required (e.g. for MPC). These conditions are not realistic for an operational WEC and inevitably performance will be degraded. A control strategy must be robust to modelling errors and other uncertainty, but also must be simple to implement for practical deployment. An appropriate solution is the Simple and Effective controller proposed in [17], whereby a computed velocity reference signal is designed to keep the WEC velocity in phase with the wave excitation while also considering physical constraints such as position limits. Velocity tracking is achieved by a feedback control loop and many architectures are suitable for this purpose. In [18] the Simple and Effective strategy is applied to a submerged multi-DOF WEC with three taut tethers using an Internal Model Control loop for velocity tracking. In [19] an adaptive strategy is applied to a 1-DOF WEC to improve performance with a highly nonlinear hydraulic PTO. Here the Simple and Effective strategy is applied to a multi-DOF point absorber. A specific WEC (WaveSub) is used to provide a meaningful study and is simulated in the WEC-Sim environment [20]. A Linear Quadratic Regulator state feedback loop is designed for velocity tracking, including full modal coupling. Performance is compared to an optimally tuned passively controlled system in a wide range of irregular sea states.

This study is distinct from others for the following reasons:

- The target WEC is not purely theoretical and idealised. A validated kinematic nonlinear model is utilised. Experimental systems up to 1:4 scale have been tested and a full scale system is under development.
- The control system is designed around a linearised model of the WEC, but is then tested with the full WEC-Sim model so modelling errors are inherent and indeed identified.
- The WEC is free to move in all six DOF, though is largely constrained to heave, surge and pitch as it is aligned with planar waves.
- Precise knowledge of the wave excitation force is not assumed. It is estimated from the modelled system dynamics using measurable quantities in a deployable system.

The remainder of the paper is arranged as follows. An overview of the WaveSub WEC is provided in section II. Descriptions of the WEC model and its linearised equivalent are provided in sections III and IV. The control strategy is described in section V with a method for wave force estimation given in section VI. Simulation results comparing the passive benchmark system performance against the actively controlled system under realistic conditions are provided in section VII. Conclusions are provided in section VIII.

79

## II. OVERVIEW OF THE WAVESUB WEC

80 WaveSub is under development by Marine Power Systems Ltd (MPS). It is a submerged point  
 81 absorber with a unique multi-tether configuration and variable geometry which can be tuned to the  
 82 prevailing sea state. A float moves with the waves and reacts against a moored base. The tethers pull  
 83 on rotational drums which are attached to a PTO. An illustration of a full scale multi-float concept  
 84 is shown in Figure 1.

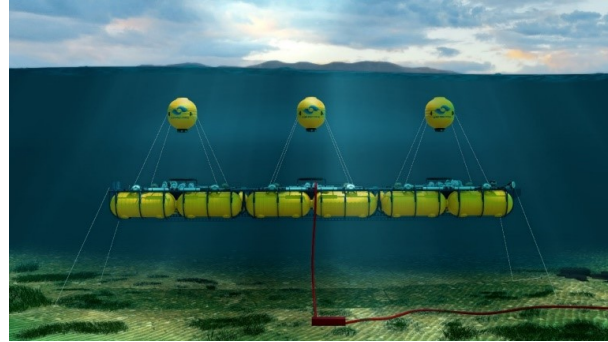


Fig. 1. Illustration of full scale multi-float WaveSub concept

85 This study uses a single section of this device, comprising a single float with four taut tethers  
 86 connected to individual drums and rotational PTOs. The block diagram of the complete system is  
 87 shown in Figure 2.

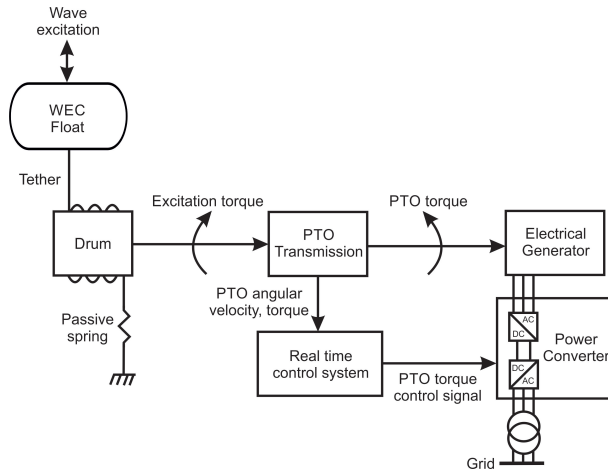


Fig. 2. Block diagram representation of WEC/PTO systems

88

## III. BASELINE WEC SIMULATION

### A. Model Description

90 A 1:25 scale WEC-Sim model of a single float system using four PTO tethers and a taut mooring  
 91 system has been validated against experimental data from wave tank testing [21]. A full-scale  
 92 WEC-Sim model has been extrapolated from the 1:25 scale model and is the subject of this study.  
 93 The optimum passive spring-damper combinations have been established across the full range  
 94 of operational irregular sea conditions and this system is used as a benchmark for performance  
 95 comparison against an actively controlled PTO system. Figure 3 shows an image of the simplified  
 96 geometry used for simulation in the WEC-Sim package. The dimensions are given in table I.

97 The float and reactor are connected with four taut PTO tether lines, each modelled as a translational  
 98 PTO actuation force incorporating a spring stiffness and damping force, a universal joint and gimbal.  
 99 All motions and forces are available for use by the control strategy within this model and the control

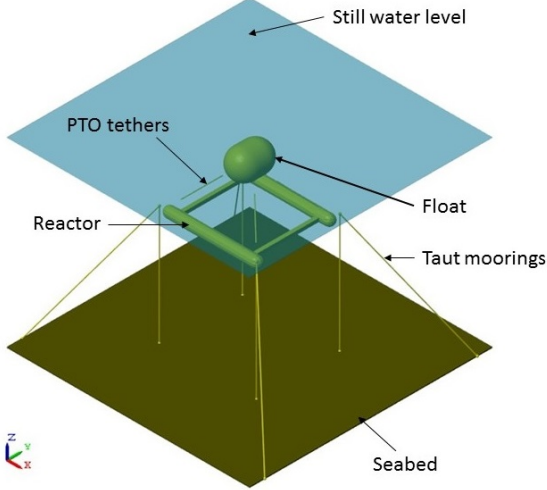


Fig. 3. Simplified geometry and mooring in WEC-Sim

TABLE I  
DIMENSIONS OF THE GEOMETRY OF THE FULL SCALE WEC-SIM MODEL

Properties	Value	Unit
Float diameter	12	m
Float cylinder length	4.75	m
Reactor length	51.55	m
Reactor width	50	m
Reactor height	4.85	m

100 force applied to each PTO is incorporated by adding to the external preload force on each PTO. The  
 101 damping force is used only for the benchmark passive optimally tuned system and is set to zero for  
 102 active control. Irregular waves are applied in the  $x$ -direction.

103 Results using a Pierson-Moskowitz (PM) spectrum with significant wave height  $H_s = 3\text{m}$  and  
 104 energy period  $T_e = 10\text{s}$  (see Figure 4) are presented in detail, giving insight into the internal signals  
 105 and processes occurring within the passive and active control systems. This sea state represents a  
 106 typical sea state for which the device is sized. A wide range of PM spectra with  $H_s = 0.5 - 6.5\text{m}$   
 107 and  $T_e = 6 - 16\text{s}$  are used latterly for mean power capture comparison. All simulations were for a  
 108 700s duration in total with a sample time of 0.02s.

#### 109 B. Forces acting on the float body

110 The float body system dynamics are governed by:

$$M\ddot{x} = F_h(t) + F_m(t) \quad (1)$$

111 where  $M$  is the float mass matrix,  $\ddot{x}$  is the float acceleration vector,  $F_h(t)$  is the total hydrodynamic  
 112 force vector and  $F_m(t)$  is the mechanical force vector of the PTO. Assuming linear wave theory, the  
 113 hydrodynamic force can be decomposed as follows:

$$F_h(t) = F_e(t) + F_r(t) + F_{hs}(t) + F_v(t) \quad (2)$$

114 where  $F_e(t)$ , is the excitation force produced by an incident wave on an otherwise fixed body,  $F_r(t)$   
 115 is the radiation force which is produced by an oscillating body creating waves on an otherwise still  
 116 sea, and  $F_{hs}(t)$  is the hydrostatic restoring force.  $F_v(t)$  is a nonlinear viscous damping term which  
 117 is commonly neglected.

118  $F_{hs}(t)$  is constant as the float is fully submerged. In the heave direction it is given by

$$F_{hs}(t) = -\rho g V \quad (3)$$

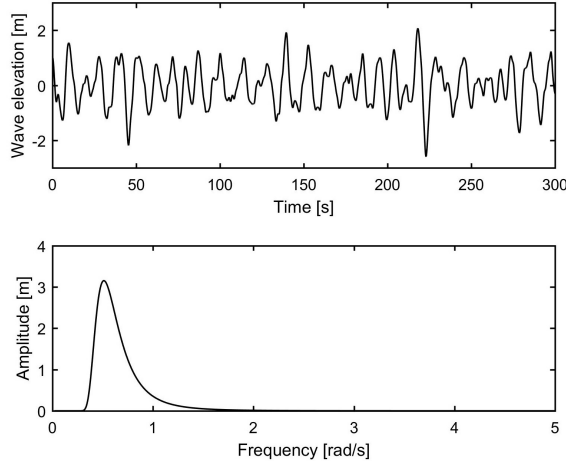


Fig. 4. Wave elevation and spectrum for irregular waves (Pierson-Moskowitz with  $H_s = 3\text{m}$   $T_e = 10\text{s}$ )

119 where  $\rho$  is the water density,  $g$  is the acceleration due to gravity and  $V$  is the float volume.  
120 The radiation force in the time domain is given by [22]

$$\mathbf{F}_r(t) = -\mathbf{A}_\infty \ddot{\mathbf{x}} - \int_0^t \mathbf{K}_r(t-\tau) \dot{\mathbf{x}}(\tau) d\tau \quad (4)$$

121 where  $\mathbf{A}_\infty$  is the infinite frequency added mass matrix,  $\mathbf{K}_r$  is the radiation impulse function and  
122  $\mathbf{x} \in R^{6 \times 1}$  is the state vector given by

$$\mathbf{x} = [x \ y \ z \ \theta_x \ \theta_y \ \theta_z]^T \quad (5)$$

123 The excitation and radiation forces are calculated using hydrodynamic coefficients computed by  
124 the NEMOH BEM solver [23].

### 125 C. Optimal tuning of PTO stiffness and damping

126 The passively damped system uses a fixed damping coefficient on each PTO, which is dependent  
127 on the peak period of the wave spectrum applied. For each sea state tested the passive damping  
128 co-efficient and spring stiffness were optimally tuned. The optimal parameters are shown in Figure 5.

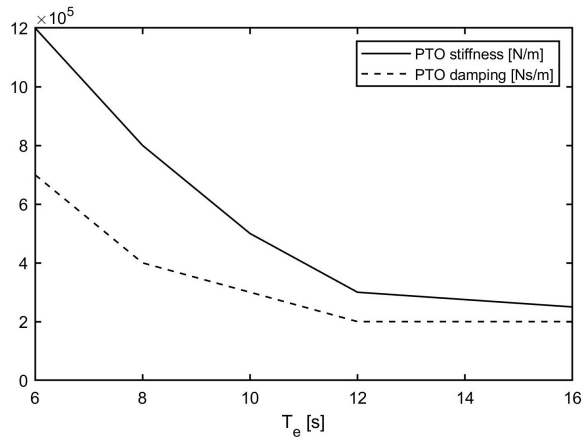


Fig. 5. Optimal stiffness and damping curves for passive WEC

129 As such the passive system benchmark performance represents the highest possible captured power  
 130 with a fixed damping coefficient in a given sea state. In practice, to achieve this, the damping  
 131 coefficient would need to vary as the incident sea state changes. This could be achieved using a  
 132 slow-tuning control strategy (e.g. [24]), but performance will degrade sharply if the damping is  
 133 poorly tuned. Tuning in operation would depend upon good estimation of the peak energy period  
 134 of the incident sea-state. This is not always possible due to long data lengths required, and the lack  
 135 of a defined peak or double peaks in some seas.

#### 136 IV. LINEARISED DYNAMIC SYSTEM MODEL

137 A linearised approximation to the WEC and PTO systems is typically required for model-based  
 138 control system design. Assuming the reactor to be fixed for simplicity (this is acceptable with the  
 139 taut mooring system) we can use the approach of [25] and [18]. The plant dynamics are represented  
 140 by the state-space system

$$\begin{aligned} \dot{\mathbf{x}}^+ &= \begin{bmatrix} \dot{\mathbf{x}} \\ \dot{\mathbf{p}}_r \end{bmatrix} = \mathbf{A}\mathbf{x}^+ + \mathbf{B}(\mathbf{F}_e + \mathbf{u}) \\ \mathbf{y} &= \mathbf{C}\mathbf{x}^+ \end{aligned} \quad (6)$$

141 where  $\mathbf{u}$  is the 6DOF control force vector and the state vector is given by  $[\mathbf{x} \ \dot{\mathbf{x}}]^T$ . The state vector is  
 142 augmented with the auxiliary states  $\mathbf{p}_r$  relating to a 4<sup>th</sup> order State-Space approximation  $\mathbf{G}_r$  of the  
 143 radiation impulse response functions described by

$$\begin{aligned} \dot{\mathbf{p}}_r &= \mathbf{A}_r \mathbf{p}_r + \mathbf{B}_r \dot{\mathbf{x}} \\ \int_0^t \mathbf{K}_r(t-\tau) \dot{\mathbf{x}}(\tau) d\tau &\approx \mathbf{C}_r \mathbf{p}_r + \mathbf{D}_r \dot{\mathbf{x}} \end{aligned} \quad (7)$$

144 where the matrices  $\{\mathbf{A}_r, \mathbf{B}_r, \mathbf{C}_r, \mathbf{D}_r\}$  describing  $\mathbf{G}_r$  are computed in the BEMIO code supplied with  
 145 WEC-Sim [20]. Including all 36 modes in the state-space model results in 144 states. Figure 6 shows  
 146 the BEM and approximated radiation impulse responses for the surge and heave modes showing  
 147 the accuracy of the fitting process.

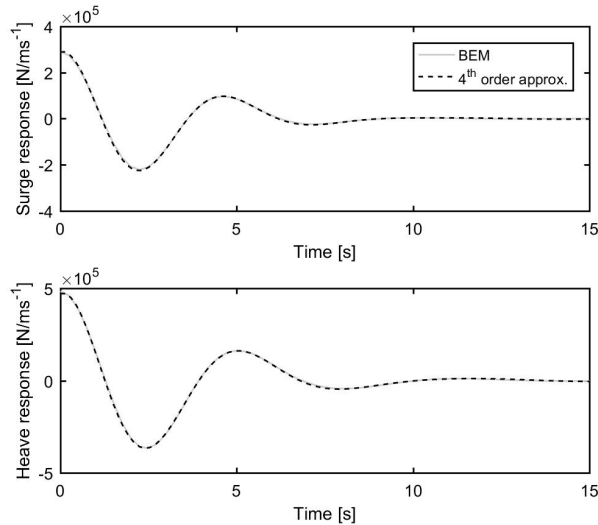


Fig. 6. Surge and heave radiation impulse responses from BEM solver and 4<sup>th</sup> order approximation

148 The augmented plant and output matrices are obtained from linearising the WEC system about  
 149 its nominal resting position. These are given by equations 8-10 where  $\mathbf{A}_\infty$  is obtained from the BEM  
 150 solution,  $\mathbf{K}_0$  is the linearised stiffness matrix (see [25]) and  $\mathbf{B}_v$  is a linear viscous damping matrix  
 151 empirically tuned to experimental data [21]. The state-space model order can be reduced by obtaining  
 152 a balanced state-space realization and eliminating states with negligible contribution to the system

153 response. Using this approach the total number of states can be reduced to 44, resulting in a model  
 154 suitable for control system design.

$$\mathbf{A} = \left[ \begin{array}{c|c} \mathbf{0}^{6 \times 6} & \mathbf{I}^{6 \times 6} \\ \hline -(\mathbf{M} + \mathbf{A}_\infty)^{-1} \mathbf{K}_0 & -(\mathbf{M} + \mathbf{A}_\infty)^{-1} (\mathbf{B}_v + \mathbf{D}_r) \\ \hline \mathbf{0}^{144 \times 6} & \mathbf{B}_r \end{array} \right] \quad (8)$$

$$\mathbf{B} = \left[ \begin{array}{c} \mathbf{0}^{6 \times 6} \\ \hline (\mathbf{M} + \mathbf{A}_\infty)^{-1} \\ \hline \mathbf{0}^{144 \times 6} \end{array} \right] \quad (9)$$

$$\mathbf{C} = [ \mathbf{0}^{6 \times 6} \quad \mathbf{I}^{6 \times 6} \quad | \quad \mathbf{0}^{6 \times 144} ] \quad (10)$$

155 Figure 7 shows the surge, heave and pitch float velocities under controlled conditions. Results  
 156 are shown for three irregular sea states with the same peak period and increasing significant wave  
 157 heights. The reduced order linearised model shows good agreement, with accuracy reducing with  
 158 increased wave height. This is to be expected as the model is linearised about its resting position  
 159 and accuracy will degrade as the PTO tether angles change for large motions.

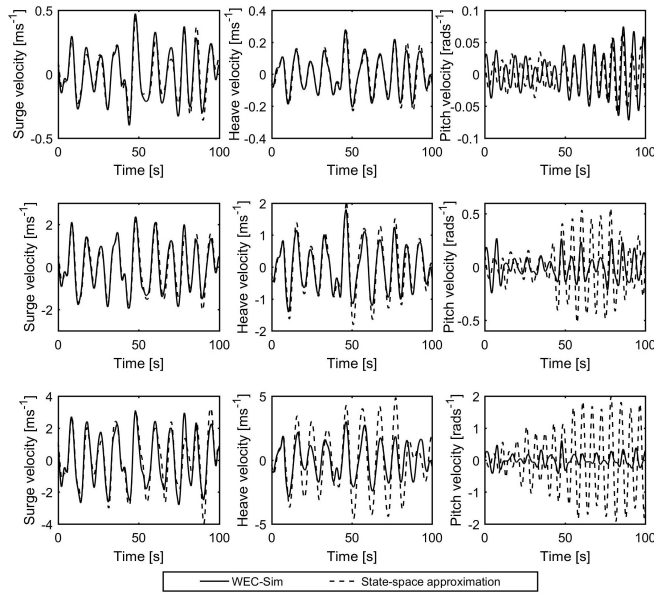


Fig. 7. Surge, heave and pitch float velocities under controlled conditions. Results shown for three sea states with  $T_e = 10$ s and  $H_s = 1\text{m}$  (TOP),  $H_s = 3\text{m}$  (MIDDLE),  $H_s = 6\text{m}$  (BOTTOM)

160

## V. ACTIVE CONTROL METHODOLOGY

161 As mentioned in section I, a practical WEC control strategy must be robust to modelling errors  
 162 and other uncertainty, but also must be simple to implement. Here we adopt the Simple and Effective  
 163 strategy proposed in [17]. A velocity reference trajectory is evolved based upon the wave excitation  
 164 force and knowledge of the plant dynamics and constraints. If the PTO can be controlled so the  
 165 float velocity tracks the reference then good power capture should be achieved. The overall control  
 166 strategy is illustrated in Figure 8.

167 The vector of Cartesian velocity reference signals is given by

$$\dot{\mathbf{x}}_{ref}(t) = \mathbf{G}^{-1}(t)\mathbf{F}_e(t) = 0.5(|\mathbf{G}_r(\hat{\omega})| + \mathbf{B}_v)^{-1}\mathbf{F}_e(t) \quad (11)$$

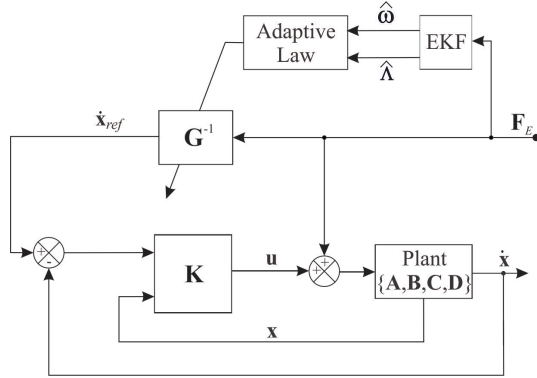


Fig. 8. Illustration of Simple and Effective control strategy with LQR velocity tracking (adapted from [17])

where  $|\mathbf{G}_r(\hat{\omega})|^{-1} \in R^{6 \times 6}$  is the inverse of a time varying matrix of the instantaneous amplitudes of the 4<sup>th</sup> order state space radiation damping model at the current estimated dominant excitation frequency  $\hat{\omega}$ .  $\mathbf{F}_e(t)$  is assumed to be a narrow band harmonic process of the form [17]

$$\mathbf{F}_e(t) = \Lambda \cos(\omega t + \phi) \quad (12)$$

It is necessary to estimate the dominant amplitude  $\hat{\Lambda}$  and frequency  $\hat{\omega}$  of the excitation force for each DOF. This is achieved using an extended Kalman Filter (EKF) as described in section VI. Linear position constraints are required to avoid impacts between the float and reactor. Position constraints are readily incorporated as a velocity constraint under the narrow band assumption and the velocity reference gain has an upper bound given by  $\bar{\mathbf{G}}^{-1} = \hat{\omega} \bar{\mathbf{x}} / \hat{\Lambda}$  where  $\{\cdot\}$  denotes elementwise multiplication or division and  $\{\cdot\}^-$  is the maximum permissible value of a quantity. Thus a real-time variable gain on the velocity reference may be expressed as

$$\mathbf{G}^{-1}(t) = \begin{cases} 0.5(|\mathbf{G}_r| + \mathbf{B}_v)^{-1} : \bar{\mathbf{G}}^{-1} \geq 0.5(|\mathbf{G}_r| + \mathbf{B}_v)^{-1} \\ \bar{\mathbf{G}}^{-1} : \text{otherwise} \end{cases} \quad (13)$$

178 In this study the waves are unidirectional in the  $x$ -direction, so only surge and heave motion need  
179 to be controlled to prescribed trajectories.

180 Tracking of the velocity reference is achieved using a Linear Quadratic Regulator (LQR) state  
 181 feedback controller under the assumption all states may be measured or accurately estimated.  $\mathbf{K}$  is  
 182 obtained from LQR optimisation to minimise the cost function

$$J(u) = \int_0^\infty (\mathbf{x}_e^T \mathbf{Q} \mathbf{x}_e + \mathbf{u}^T \mathbf{R} \mathbf{u}) dt \quad (14)$$

<sup>183</sup> where  $\mathbf{x}_e$  is the error state trajectory given by

$$\mathbf{x}_e = \begin{bmatrix} \mathbf{0}^{6 \times 1} \\ \dot{\mathbf{x}}_{ref} \end{bmatrix} - \begin{bmatrix} \mathbf{x} \\ \dot{\mathbf{x}} \end{bmatrix} \quad (15)$$

184 The resulting state feedback gain is

$$\mathbf{K} = \mathbf{R}^{-1} \mathbf{B}^T \mathbf{S} \quad (16)$$

<sup>185</sup> where  $\mathbf{S}$  is the solution to the algebraic Riccati equation

$$\mathbf{A}^T \mathbf{S} + \mathbf{S} \mathbf{A} - \mathbf{S} \mathbf{B} \mathbf{R}^{-1} \mathbf{B}^T \mathbf{S} + \mathbf{Q} = 0 \quad (17)$$

<sup>186</sup> and the weighting matrices are designed to balance control effort against tracking performance.  
<sup>187</sup> Similar to [26], for  $\mathbf{Q}$  we choose

$$\mathbf{Q} = \mathbf{C}^T \bar{\mathbf{Q}} \mathbf{C} \quad (18)$$

188 where  $\bar{\mathbf{Q}} \in R^{6 \times 6}$  is the auxiliary output error weighting matrix given by

$$\bar{\mathbf{Q}} = \frac{\bar{T}}{\bar{v}^2} \begin{bmatrix} |diag([\mathbf{e}_{si}])| & \mathbf{0}^{3 \times 3} \\ \mathbf{0}^{3 \times 3} & r.|diag(\mathbf{F}_i \times \mathbf{e}_{si})| \end{bmatrix} \quad (19)$$

189 where  $T$  and  $v$  are the PTO tether tension and velocity respectively, and  $r$  is the radius of the float.  
190 With reference to Figure 9,  $\mathbf{F}_i$  is the the float connection point coordinate vector relative to the float  
191 centre of gravity and  $\mathbf{e}_{si}$  is the unit vector along the direction of the  $i^{th}$  PTO tether in the nominal  
192 WEC position. As the system has  $x - y$  symmetry it does not matter which tether is used.

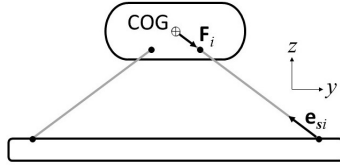


Fig. 9. Illustration of WEC kinematics

193 The control effort weighting is chosen as

$$\mathbf{R} = \frac{1}{\bar{T}} diag [\rho_1 \ \rho_2 \ \dots \ \rho_6] \quad (20)$$

194 with  $\rho_i$  chosen appropriately to weight control effort in each DOF and achieve good tracking  
195 performance.

196 The control law in Cartesian coordinates is given as

$$\mathbf{u} = -\mathbf{K}\mathbf{x}_e \quad (21)$$

197 Distribution of  $\mathbf{u}(t)$  to the four PTOs is achieved according to

$$\mathbf{u}_{PTO} = \mathbf{J}_0^T \mathbf{u} \quad (22)$$

198 where  $\mathbf{J}_0^{-1}$  is the inverse kinematic Jacobian matrix given by [27]

$$\mathbf{J}_0^{-1} = \begin{bmatrix} \mathbf{e}_{s1}^T & (\mathbf{F}_1 \times \mathbf{e}_{s1})^T \\ \vdots & \vdots \\ \mathbf{e}_{s4}^T & (\mathbf{F}_4 \times \mathbf{e}_{s4})^T \end{bmatrix} \quad (23)$$

199

## 200 VI. ESTIMATION OF WAVE EXCITATION FORCE

201 The wave excitation or disturbance force is not measurable, but is required for the proposed control  
202 strategy. In order to estimate the disturbance force it is required to know the dynamics of the float  
203 body and all other forces acting upon it, as well as estimates or measurements of the float motion.  
204 Float motion and all forces other than the excitation force are readily measured or estimated as  
205 previously described. It this then possible to implement a dynamic observer to estimate the wave  
206 excitation force. Here we use a combination of Kalman Filter approaches. First, we use the method  
207 described in [28], to estimate the excitation force. Then this is combined with the Extended Kalman  
208 filter described in [29] to estimate the instantaneous amplitude and frequency of the estimated  
209 excitation force for use in the real-time controller. As we are able to measure the tether forces directly  
210 using load cells, we can directly measure the combination of control force and passive spring force.

211 The state vector  $\mathbf{x}^+$  is further augmented with the unknown disturbance force  $\mathbf{F}_e$  and its time-  
212 varying cyclical amplitude and frequency vectors  $\Psi = [\Lambda \ \Lambda^* \ \omega]$  for each relevant degree-of-freedom.

<sup>213</sup> Maintaining the notation  $\mathbf{x}^+$  for the further augmented state vector for convenience, the discretized  
<sup>214</sup> system dynamics are now described by

$$\mathbf{x}_{k+1}^+ = \begin{bmatrix} \mathbf{x}^+ \\ \mathbf{F}_e \\ \Psi_1 \\ \vdots \\ \Psi_n \end{bmatrix}_{k+1} = \mathbf{A}^+ \mathbf{x}_k^+ + \mathbf{B}^+ (\mathbf{F}_e - \mathbf{F}_{PTO})_k + \boldsymbol{\epsilon}_k \quad (24)$$

$$\mathbf{y} = \mathbf{C}^+ \mathbf{x}_k^+ + \boldsymbol{\mu}_k$$

<sup>215</sup> where  $\boldsymbol{\epsilon}$  describes the random walk process for excitation force estimation and unmodelled dynamics,  
<sup>216</sup> and  $\boldsymbol{\mu}$  describes measurement noise.  $\mathbf{F}_{PTO}$  is the Cartesian vector of tether tension forces, derived  
<sup>217</sup> from direct measurement of the combined control and spring forces according to

$$\mathbf{F}_{PTO} = \mathbf{J}_0^{-T} (\mathbf{u}_{PTO} + \mathbf{K}_o \mathbf{x}) \quad (25)$$

<sup>218</sup> where  $\mathbf{J}_0^{-T}$  is the transpose of the inverse kinematic Jacobian matrix. The system matrices are  
<sup>219</sup> defined as follows:

$$\mathbf{A}^+ = \begin{bmatrix} \mathbf{A} & \mathbf{B} & \mathbf{0} & \mathbf{0} & \mathbf{0} \\ \mathbf{0} & \mathbf{I} & \mathbf{0} & \mathbf{0} & \mathbf{0} \\ \mathbf{0} & \mathbf{0} & \mathbf{A}_1^c & \mathbf{0} & \mathbf{0} \\ \mathbf{0} & \mathbf{0} & \mathbf{0} & \ddots & \mathbf{0} \\ \mathbf{0} & \mathbf{0} & \mathbf{0} & \mathbf{0} & \mathbf{A}_n^c \end{bmatrix} \quad \mathbf{B}^+ = \begin{bmatrix} \mathbf{B} \\ \mathbf{0} \\ \mathbf{0} \end{bmatrix} \quad (26)$$

$$\mathbf{C}^+ = \begin{bmatrix} \mathbf{C} & \mathbf{D} & \mathbf{0} \\ \mathbf{0} & \mathbf{0} & (1 & 0 & 0) & \mathbf{0} & \mathbf{0} & \mathbf{0} & \mathbf{0} \\ \mathbf{0} & \mathbf{0} & \mathbf{0} & \mathbf{0} & \mathbf{0} & \ddots & \mathbf{0} & \mathbf{0} & \mathbf{0} \\ \mathbf{0} & \mathbf{0} & \mathbf{0} & \mathbf{0} & \mathbf{0} & \mathbf{0} & (1 & 0 & 0) \end{bmatrix}$$

<sup>220</sup> where, for the  $i^{th}$  degree of freedom,

$$\mathbf{A}_i^c = \begin{bmatrix} \cos\omega_i\Delta t & \sin\omega_i\Delta t & 0 \\ -\sin\omega_i\Delta t & \cos\omega_i\Delta t & 0 \\ 0 & 0 & 1 \end{bmatrix} \quad (27)$$

<sup>221</sup> where  $\Delta t$  is the sampling interval and  $\{\mathbf{A}, \mathbf{B}, \mathbf{C}\}$  are as per equations 8 to 10 but with the stiffness  
<sup>222</sup> matrix  $\mathbf{K}_0$  set to  $0^{6 \times 1}$  as this force is measured.

<sup>223</sup> The prediction step estimates the next state  $\hat{\mathbf{x}}_{k|k-1}^+$  and covariance  $\mathbf{P}_{k|k-1}^+$  matrices as:

$$\begin{aligned} \hat{\mathbf{x}}_{k|k-1}^+ &= \mathbf{A}_{k-1}^+ \hat{\mathbf{x}}_{k-1|k-1}^+ + \mathbf{B}^+ \mathbf{F}_{PTO,k-1|k-1} \\ \mathbf{P}_{k|k-1}^+ &= \mathbf{J}_{k-1}^+ \mathbf{P}_{k-1|k-1}^+ \mathbf{J}_{k-1}^{+T} + \mathbf{Q}_{k-1}^+ \end{aligned} \quad (28)$$

<sup>224</sup> where  $\mathbf{Q}^+$  is the process noise covariance matrix, assumed to represent a zero mean Gaussian  
<sup>225</sup> process. The update step is defined by:

$$\begin{aligned} \mathbf{S}_k^+ &= \mathbf{C}_k^+ \mathbf{P}_k^+ \mathbf{C}_k^{+T} + \mathbf{R}_k^+ \\ \mathbf{K}_k^+ &= \mathbf{P}_k^+ \mathbf{C}_k^{+T} \mathbf{S}_k^{+-1} \\ \hat{\mathbf{x}}_{k|k}^+ &= \hat{\mathbf{x}}_{k|k-1}^+ + \mathbf{K}_k^+ \left( [\mathbf{y}_k \quad \hat{\mathbf{F}}_e]^T - \mathbf{C}_k^+ \hat{\mathbf{x}}_{k|k-1}^+ \right) \\ \mathbf{P}_{k|k}^+ &= (I - \mathbf{K}_k^+ \mathbf{C}_k^+) \mathbf{P}_{k|k-1}^+ \end{aligned} \quad (29)$$

<sup>226</sup> where  $\mathbf{S}^+$  is the innovation residual,  $\mathbf{R}^+$  is the observation covariance associated with the observed  
<sup>227</sup> value  $\mathbf{y}$ , and  $\mathbf{K}$  is the Kalman gain.  $\mathbf{J}^+$  is the Jacobian of  $\mathbf{A}^+$  which is recalculated every time step  
<sup>228</sup> as  $\mathbf{A}^c$  is time-varying.

<sup>229</sup> Figure 10 shows good estimation of the excitation force for surge and heave directions.

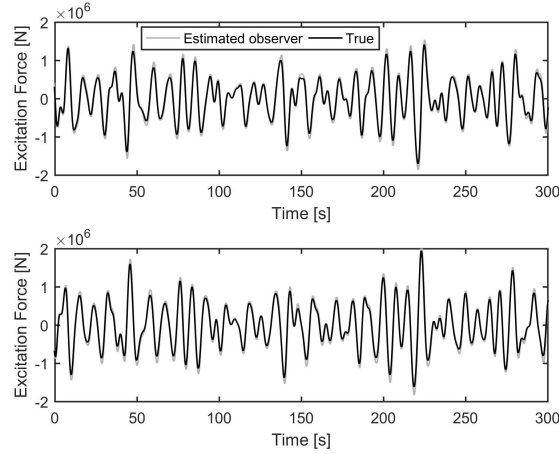


Fig. 10. Estimation of wave excitation force in surge and heave directions in irregular waves (Pierson-Moskowitz with  $H_s = 3\text{m}$ ,  $T_e = 10\text{s}$ )

230     Figure 11 shows the amplitude and frequency estimation of an observed signal for the wave  
 231    excitation force in surge and heave for irregular waves obtained from the Wec-Sim simulation. Good  
 232    estimation of instantaneous amplitude and frequency is achieved.

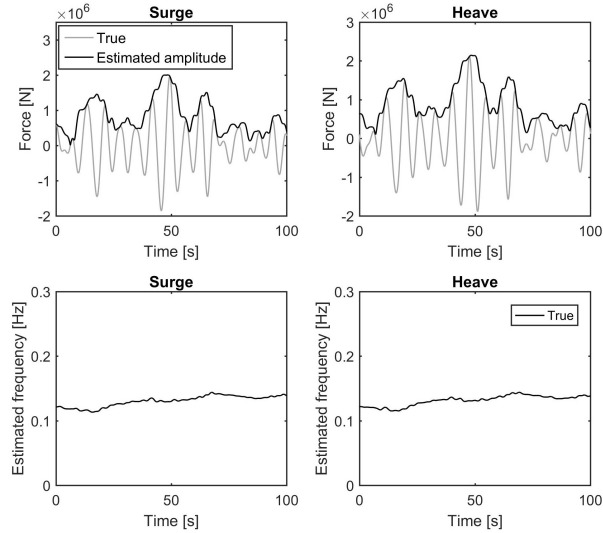


Fig. 11. EKF wave force amplitude and frequency estimation

233

## VII. SIMULATION RESULTS

234     For detailed insight into the actively controlled system performance, the irregular sea-state of  
 235    Figure 4 was imposed upon the full nonlinear WEC-Sim model.

236    A. Velocity reference tracking

237     Figure 12 shows the surge and heave reference and measured float velocities. An achievable  
 238    velocity reference signal has been generated and the active control strategy is clearly seen to provide  
 239    good tracking.

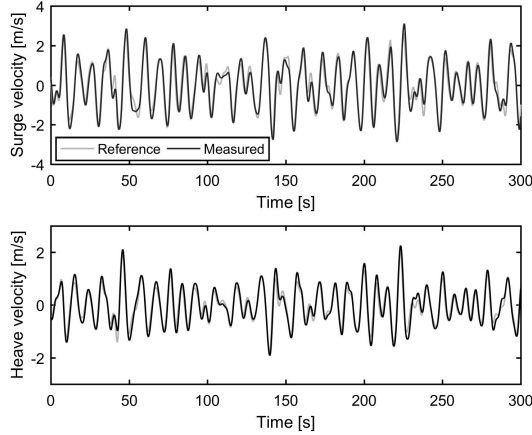


Fig. 12. Surge and heave reference and measured float velocities under controlled conditions (sea state  $H_s = 3\text{m}$ ,  $T_e = 10\text{s}$ ) for full WEC-Sim model

240 Displacement limits from nominal of  $\pm 5\text{m}$  in surge and  $\pm 3\text{m}$  in heave were imposed. Figure 13  
 241 shows that the displacement limits are largely adhered to. These limits are imposed in a soft manner,  
 242 so a factor of safety can be applied if it is critical that they are not exceeded. Though it is not  
 243 controlled, the pitch motion is included for completeness. Also shown are the motions under passive  
 244 control for comparative purposes.

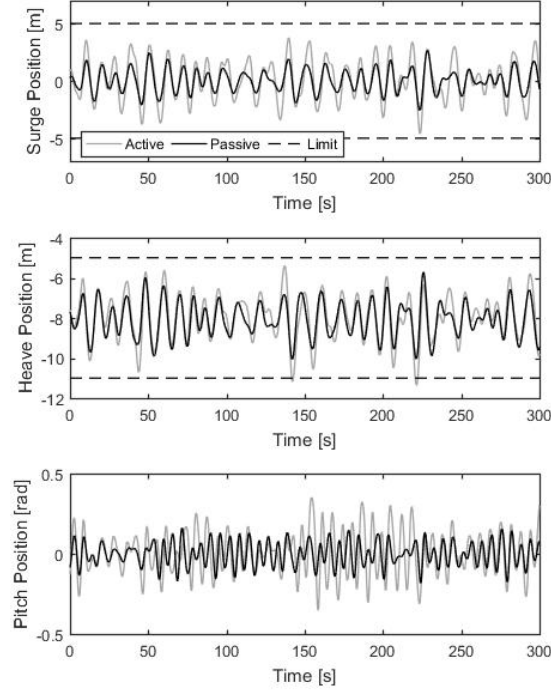


Fig. 13. Surge, heave and pitch float positions under controlled conditions (sea state  $H_s = 3\text{m}$ ,  $T_e = 10\text{s}$ ) for full WEC-Sim model

245 *B. Load limiting*

246 Figure 14 shows the % increase in peak PTO tether tension for the actively controlled system  
 247 compared to the passively controlled benchmark for irregular sea states with different significant  
 wave heights.

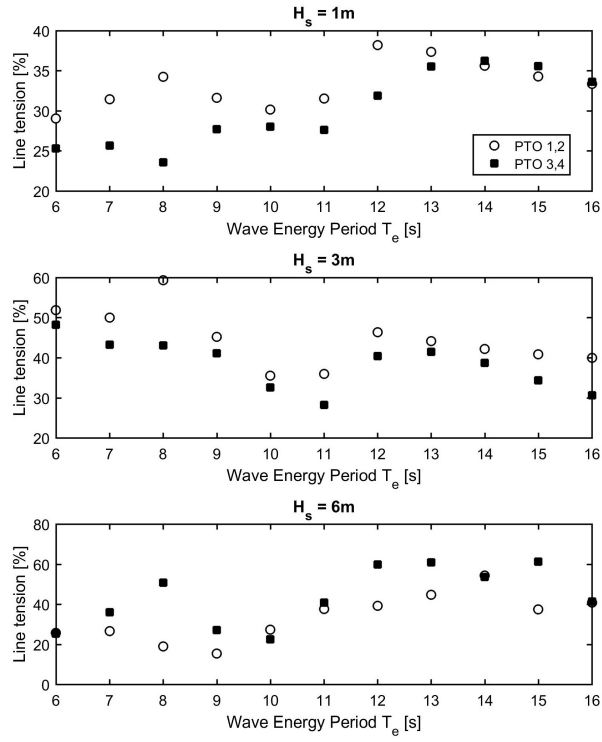


Fig. 14. % increase in peak PTO tether tension for active compared to passive control for full WEC-Sim model. Results shown for irregular sea states with a range of  $T_e$  and  $H_s = 1\text{m}$  (TOP),  $H_s = 3\text{m}$  (MIDDLE),  $H_s = 6\text{m}$  (BOTTOM)

248 The peak tether tensions are larger for the actively controlled system as expected, being up to 60%  
 249 higher than the passive system peak values. Figure 15 shows the applied PTO control forces and  
 250 the resulting PTO tether tensions which are the combination of the control force, pre-tension and  
 251 spring force. If the control force is not constrained the tether tensions are seen to become positive  
 252 occasionally. In larger seas this effect would be more prevalent. In reality this is not possible and the  
 253 PTO tethers would become slack, causing issues for controllability and potentially resulting in large  
 254 snatching loads being transmitted which would reduce the lifetime of the WEC and PTO. Therefore  
 255 it is necessary to introduce a dynamic saturation constraint on  $\mathbf{u}$ , such that  $\Delta\mathbf{u} \leq \mathbf{T}$ , where  $\Delta\mathbf{u}$  is the  
 256 change in control force from the current time step and  $\mathbf{T}$  is the vector of measured tether tensions.  
 257 Figure 15 also shows the control forces and line tensions using this constraint, it can be seen that  
 258 the tethers remain taught.

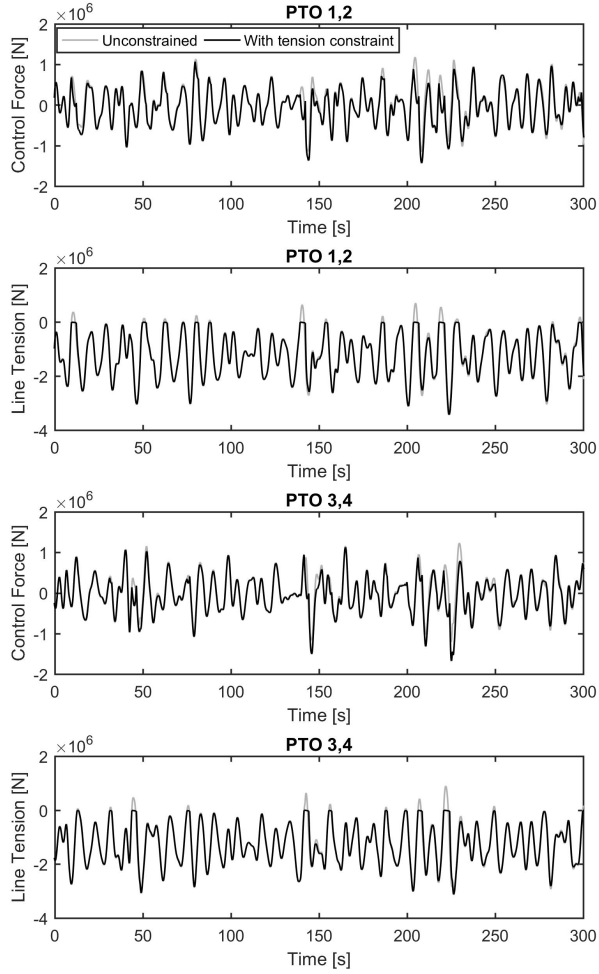


Fig. 15. Control forces and tether tensions under controlled conditions (sea state  $H_s = 3\text{m}$ ,  $T_e = 10\text{s}$ ) for full WEC-Sim model

### 260 C. Power capture

261 Figure 16 shows the instantaneous and mean generated power for the passive and actively  
 262 controlled systems. Increased power is clearly seen for the actively controlled system, though it would  
 263 also require more smoothing than the passively controlled output. The reactive power component  
 264 is clearly seen as negative power when the controller commands a motoring action from the PTOs.  
 265 This is not always possible or desirable due to the increased cost and complexity of components.  
 266 Two-quadrant operation may be favourable in many situations, and operates as a restriction of  
 267 uni-directional power flow i.e. the generator can only generate in both directions, motoring is  
 268 not permitted. This restriction may be readily incorporated to the active control strategy. This will  
 269 impact on system performance, but the benefits come in the form of reduced cost and complexity  
 270 of the components required to achieve the PTO power generation. Alternatively, it has been shown  
 271 in [30] that the reactive power requirement can be provided in the Power Electronic Converter using  
 272 supercapacitor short term energy storage.

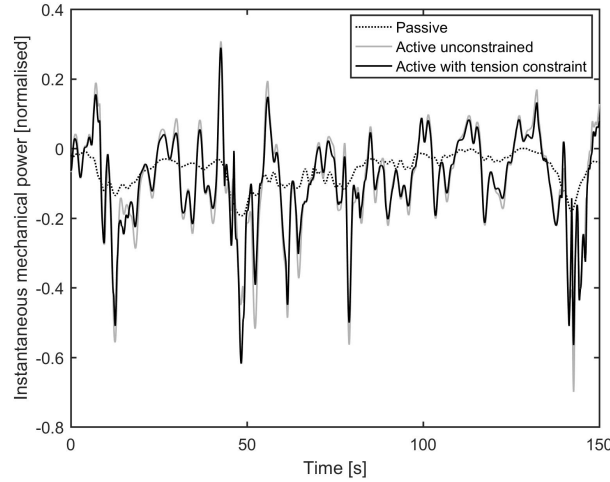


Fig. 16. Instantaneous power under controlled conditions (sea state  $H_s = 3\text{m}$ ,  $T_e = 10\text{s}$ ) for full WEC-Sim model

273     Figure 17 shows the percentage increase in mean power generation achieved by the actively  
 274     controlled system over 700s of simulation with the full nonlinear WEC-Sim model. The results are  
 275     shown for irregular PM spectra with  $H_s = 0.5 - 6.5\text{m}$  and  $T_e = 6 - 16\text{s}$ , with and without the control  
 276     force constraint. Power gains of up to 80% are observed across a wide range of irregular sea states  
 277     compared to the passive system. A slight reduction in power is seen with the control force constraint  
 278     active.

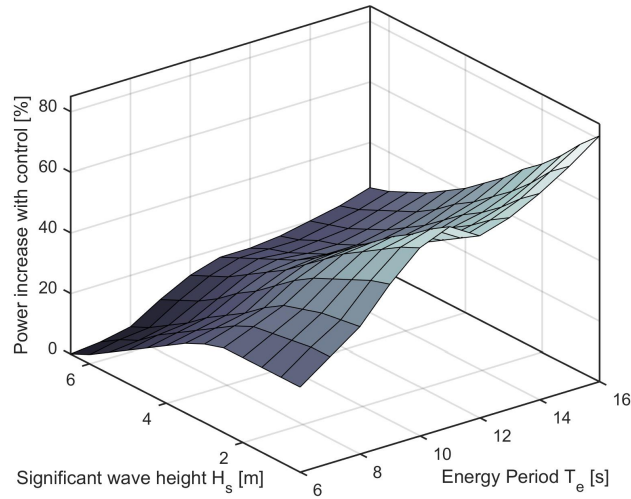


Fig. 17. Power matrix showing power percentage increase compared to optimal passive benchmark system for a range of irregular seas with peak period  $T_e$  and significant wave height  $H_s$

279     It is important to note that all performance gains reported here are relative to the optimally tuned  
 280     passive system. This means that the passive system damping coefficient was individually tailored  
 281     to a given sea state. The power capture of the passive system is very sensitive to this damping  
 282     coefficient, and large power reductions would be seen for a detuned system. The passive system  
 283     damping coefficient would need to be adjusted in service based upon the peak period of the sea state  
 284     estimated from measurement. This process is subject to errors, particularly for sea states with multiple  
 285     peaks. Therefore the performance benefits of the actively controlled system would be expected to be

286 greater in a deployed system, as it is not reliant on such measurements and the inherent uncertainty  
287 associated with them.

## VIII. CONCLUSIONS

An active control strategy has been designed for multi-DOF WECs. A velocity reference vector is calculated from the estimated wave excitation force, taking into account displacement constraints. Velocity tracking is achieved using a coupled Linear Quadratic Regulator state feedback loop with the state and control weighting matrices tuned to balance tracking performance with control effort. A load limiting constraint on the control force is applied to avoid snatching loads resulting from slack PTO tethers. The Marine Power Systems WaveSub WEC has been used as a target device to make a meaningful study. The system is modelled in the WEC-Sim environment and an optimally tuned passively damped configuration has been used as a performance benchmark. The passive and actively controlled systems were tested in WEC-Sim with a range of PM irregular sea states. Excellent performance is observed for the actively controlled system and mean power increases of up to 80% are seen compared to the optimal passive system. The control strategy does not rely on forecasting the wave excitation force many seconds into the future and is robust to parameter uncertainty. This approach shows promise to provide a substantial increase in power capture for a minimal additional device cost and therefore a significant improvement in cost of energy would likely result.

## REFERENCES

- [1] Carbon Trust technical report. UK Wave Energy Resource. 2012.

[2] R C T Rainey. Key features of wave energy. *Philosophical transactions. Series A, Mathematical, physical, and engineering sciences*, 370:425–38, 01 2012.

[3] J. Falnes. A review of wave-energy extraction. *Marine Structures*, 20:185–201, 2007.

[4] A. Babarit, G. Duclos, and A.H. Clément. Comparison of latching control strategies for a heaving wave energy device in random sea. *Applied Ocean Research*, 26(5):227–238, 2005.

[5] A.F.O. Falcão. Modelling and control of oscillating-body wave energy converters with hydraulic power take-off and gas accumulator. *Ocean Engineering*, 24:2021–2032, 2007.

[6] A.F.O. Falcão. Phase control through load control of oscillating-body wave energy converters with hydraulic PTO system. *Ocean Engineering*, 35:358–366, 2008.

[7] J.A.M. Cretel, G. Lightbody, G.P. Thomas, and A.W. Lewis. Maximisation of energy capture by a wave-energy point absorber using model predictive control. In *Proceedings of the 18th IFAC World Congress*, volume 44, pages 3714 – 3721, Milan, Italy, 2011.

[8] J. Hals, J. Falnes, and T. Moan. Constrained optimal control of a heaving buoy wave-energy converter. *Journal of Offshore Mechanics and Arctic Engineering*, 133(1):011401–011401, 2010.

[9] G. Bacelli, J.V. Ringwood, and J-C. Gilloteaux. A control system for a self-reacting point absorber wave energy converter subject to constraints. In *Proceedings of the 18th IFAC World Congress*, volume 44, pages 11387 – 11392, Milian, Italy, 2011.

[10] M. Richter, M. E. Magana, O. Sawodny, and T. K. A. Brekken. Nonlinear model predictive control of a point absorber wave energy converter. *IEEE Transactions on Sustainable Energy*, 4(1):118–126, 2013.

[11] Romain Genest and John V. Ringwood. A critical comparison of model-predictive and pseudospectral control for wave energy devices. *Journal of Ocean Engineering and Marine Energy*, 2(4):485–499, Nov 2016.

[12] O. Abdelkhalik, S. Zou, R. D. Robinett, G. Bacelli, D. G. Wilson, R. Coe, and U. Korde. Multiresonant feedback control of a three-degree-of-freedom wave energy converter. *IEEE Transactions on Sustainable Energy*, 8(4):1518–1527, Oct 2017.

[13] O. Abdelkhalik, S. Zou, G. Bacelli, D. G. Wilson, and R. Coe. Control of three degrees-of-freedom wave energy converters using pseudo-spectral methods. *ASME. J. Dyn. Sys., Meas., Control*, 140(7), 2018.

[14] D.V. Evans, D.C. Jeffrey, S.H. Salter, and J.R.M. Taylor. Submerged cylinder wave energy device: theory and experiment. *Applied Ocean Research*, 1(1):3 – 12, 1979.

[15] S. Crowley, R. Porter, and D. V. Evans. A submerged cylinder wave energy converter. *Journal of Fluid Mechanics*, 716:566–596, 2013.

- [16] S. S. Ngu, D. G. Dorrell, and E. Acha. Control of a bristol cylinder for wave energy generation. In *The 2010 International Power Electronics Conference - ECCE ASIA* -, pages 3196–3203, June 2010.
- [17] F. Fusco and J. V. Ringwood. A simple and effective real-time controller for wave energy converters. *IEEE Transactions on Sustainable Energy*, 4(1):21–30, 2013.
- [18] N. Sergienko, B. Cazzolato, P. Hardy, B. Ding, and M. Arjomandi. Internal-model-based velocity tracking control of a submerged three-tether wave energy converter. In *Proceedings of the Twelfth European Wave and Tidal Energy Conference*, Cork, Ireland, 2017.
- [19] A.J. Hillis, J. Roesner, N.P. Sell, D.R.S. Chadel, and A.R. Plummer. Investigation of the benefits of adaptive control applied to the nonlinear CCell wave energy converter. In *Proceedings of the Twelfth European Wave and Tidal Energy Conference*, Cork, Ireland, 2017.
- [20] Y. Yu, M. Lawson, K. Ruehl, and C. Michelen. Development and demonstration of the wec-sim wave energy converter simulation tool. In *Proceedings of the 2nd Marine Energy Technology Symposium, Seattle, WA*, 2014.
- [21] E. Faraggiana, C. Whitlam, John Chapman, A.J. Hillis, J. Roesner, M. Hann, D. Greaves, Y.-H. Yu, K. Ruehl, I. Masters, G. Foster, and G. Stockman. Computational modelling and experimental tank testing of the multi float wavesub under regular wave forcing. *under review with Renewable Energy*.
- [22] W. E. Cummins. The Impulse Response Function and Ship Motions. *Schiffstechnik*, 9:101–109, 1962.
- [23] A. Babarit and G. Delhommeau. Theoretical and numerical aspects of the open source BEM solver NEMOH. In *Proceedings of the 11th European Wave and Tidal Energy Conference*, Nantes, France, 2015.
- [24] C.J. Cargo, A.J. Hillis, and A.R. Plummer. Strategies for active tuning of wave energy converter hydraulic power take-off mechanisms. *Renewable Energy*, 94:32 – 47, 2016.
- [25] J.T. Scruggs, S.M. Lattanzio, A.A. Taflanidis, and I.L. Cassidy. Optimal causal control of a wave energy converter in a random sea. *Applied Ocean Research*, 42:1 – 15, 2013.
- [26] G. Vissio, D. Valério, G. Bracco, P. Beirão, N. Pozzi, and G. Mattiazzo. Iswec linear quadratic regulator oscillating control. *Renewable Energy*, 103:372 – 382, 2017.
- [27] N.Y. Sergienko, A. Rafiee, B.S. Cazzolato, B. Ding, and M. Arjomandi. Feasibility study of the three-tether axisymmetric wave energy converter. *Ocean Engineering*, 150:221 – 233, 2018.
- [28] H-N. Nguyen and P. Tona. Wave excitation force estimation for wave energy converters of the point-absorber type. *IEEE Transactions on Control Systems Technology*, 26(6):2173–2181, Nov 2018.
- [29] F. Fusco and J. V. Ringwood. Short-term wave forecasting for real-time control of wave energy converters. *IEEE Transactions on Sustainable Energy*, 1(2):99–106, July 2010.
- [30] A.J. Hillis, A.R. Plummer, X. Zeng, and J. Chapman. Simulation of a power electronic conversion system with short-term energy storage for actively controlled wave energy converters. In *Proceedings of the 6th Offshore Energy and Storage Summit*, Brest, France, 2019.